

Photonic orbital angular momentum transfer and magnetic skyrmion rotation

Wenrui Yang, Huanhuan Yang, Yunshan Cao,* and Peng Yan†

School of Electronic Science and Engineering and State Key Laboratory of Electronic Thin Film and Integrated Devices, University of Electronic Science and Technology of China, Chengdu 610054, China

Magnetic skyrmions are chiral quasiparticles that show promise for future spintronic applications such as skyrmion racetrack memories and logic devices because of their topological stability, small size (typically $\sim 3 - 500$ nm), and ultralow threshold force to drive their motion. On the other hand, the ability of light to carry and deliver orbital angular momentum (OAM) in the form of optical vortices has attracted a lot of interest. In this work, we predict a photonic OAM transfer effect, by studying the dynamics of magnetic skyrmions subject to Laguerre-Gaussian optical vortices, which manifests a rotational motion of the skyrmionic quasiparticle around the beam axis. The topological charge of the optical vortex determines both the magnitude and the handedness of the rotation velocity of skyrmions. In our proposal, the twisted light beam acts as an optical tweezer to enable us displacing skyrmions over large-scale defects in magnetic films to avoid being captured.

I. INTRODUCTION

A skyrmion is a swirling noncoplanar texture originally introduced by Skyrme a half century ago, as a hypothetical particle in the baryon theory [1], and later was observed in many condensed matter systems, such as liquid crystals, superfluids, and chiral magnets. The magnetic skyrmion, a topologically protected spin texture with a quantized topological charge [2–8], has been a prominent topic of spintronics since the first experimental observations of skyrmion lattices in bulk noncentrosymmetric magnets [9, 10] and thin films [11]. Depending on the magnetization rotation, three distinct types of skyrmions have been observed experimentally, referred to as Néel skyrmion, Bloch skyrmion and antiskyrmion [12]. The manipulation of skyrmions is of great importance and interest: skyrmions can be driven by spin-polarized current [13–17], magnetic field or electric-field gradients [18–20], temperature gradients [21–23], and spin waves [24–27]. However, the genuine skyrmion Hall effects [28, 29] tend to result in skyrmion accumulations at the edge of devices, although strongly coupled bilayer-skyrmions [30] were proposed hopefully to overcome the problem. Crystal imperfections [31, 32] on the other hand may capture or stop skyrmions. These difficulties hinder the precise manipulation of the skyrmion motion by the mentioned control methods. Thus, it should be very interesting and important if one can find other effective control methods and principles to manipulate skyrmions in magnetic thin films.

Since the theoretical work of Poynting [33] and the experiments by Beth [34, 35], it has been known that light can carry angular momentum that is associated with circular polarization and arises from the spin of individual photons and is termed spin angular momentum. Following the pioneering work by Allen *et al.* [36], it was realized that light can also carry orbital angular momentum (OAM) with helical phase fronts characterized by an $\exp(il\varphi)$ azimuthal phase dependence. Such twisted lights have a phase dislocation on the axis that is sometimes referred to as an optical vortex [37]. The OAM in the light propagation direction has the discrete value of $\hbar l$ per photon. Integer l is called the topological charge of the twisted photon. A number of demonstrations and applications of twisted lights have been brought forward [38]. They range from optical data storages to quantum communications, and black holes, among others [39–42]. Optical vortices with high OAM have been achieved using spiral phase plates, computer-generated holograms, mode conversions, spatial light modulators, etc. Very recently, OAM quantum number up to 10,010 by means of spiral phase mirrors was reported [43].

In this work, we let skyrmions enter the field of OAM. We theoretically propose to use Laguerre-Gaussian (LG) optical vortices to manipulate the skyrmion dynamics via the OAM transfer. A rotational motion of an isolated skyrmion is found (see Fig. 1). We show that the topological charge l of the optical vortex plays a key role in driving the skyrmion motion: a positive l brings about an anticlockwise rotation of skyrmions around the beam axis, while a negative l results in a clockwise one. Finally, we demonstrate that optical vortices like tweezers can grip a skyrmion to overfly large-scale defects in magnetic films to avoid being captured.

II. LAGUERRE-GAUSSIAN BEAM AND OAM TRANSFER

The twisted light beam with LG mode is a special solution of Maxwell's Eqs. under the paraxial approximation for electromagnetic waves in vacuum. At the focal plane $z = 0$, the vortex magnetic field is given by [36]

$$\mathbf{B}_{n,l}(\rho, \varphi, t) = B_0 \frac{\left(\frac{\rho}{w}\right)^{|l|} e^{-\frac{\rho^2}{w^2}} L_n^{|l|}\left(\frac{2\rho^2}{w^2}\right)}{\sqrt{w}} e^{i(\omega t - l\varphi)} \mathbf{e}_\rho, \quad (1)$$

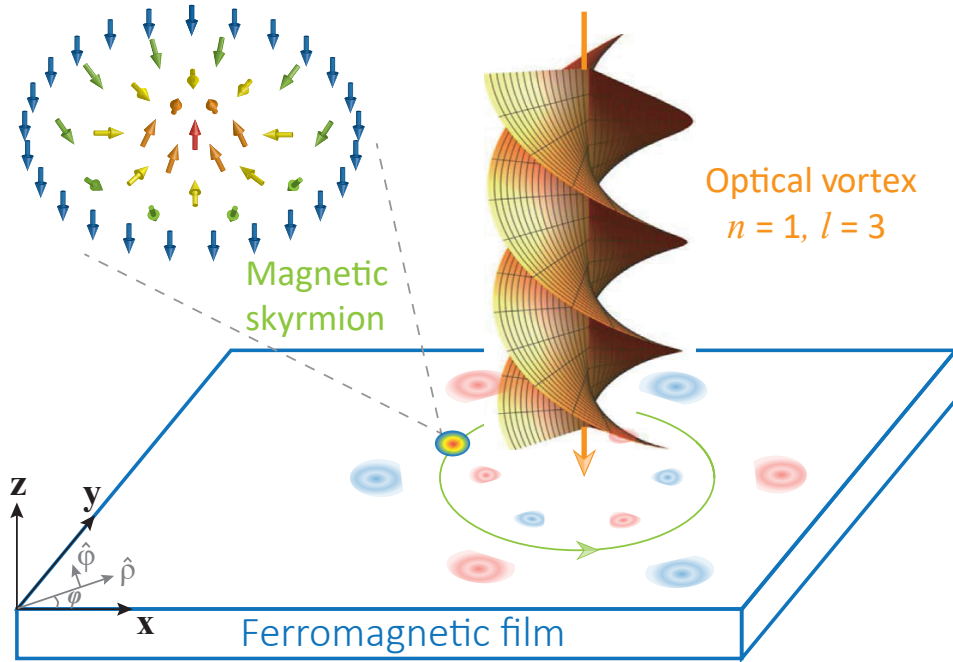


FIG. 1: Schematic of the rotational motion of a Néel skyrmion in a thin ferromagnetic film driven by an optical vortex with radial index $n = 1$ and OAM quantum number $l = 3$. The solid circle with a red core represents the skyrmion. The flower-like pattern (pink and blue spots) sketches the induced magnetization profile by the optical vortex field shining on the magnetic film. In the main text, the origin of Cartesian coordinates coincides with the beam center, while it does not in the figure for clarity.

in the cylindrical coordinate (ρ, φ, z) with the radial coordinate ρ , the azimuthal angle φ , and the coordinate z along the wave propagation direction (Fig. 1). Here w is the width of the beam waist, B_0 is a constant, L_n^l is the generalized Laguerre function, and \mathbf{e}_p is the polarization vector. Two integers n and l denote the radial index and OAM quantum number [44], respectively. In this work, we focus on linearly polarized lights and assume $\mathbf{e}_p = \mathbf{x}$.

Optical vortex can transfer its OAM to skyrmions via a coherent Zeeman coupling between photon magnetic fields and local magnetic moments. One thus expect a skyrmion rotation after it absorbs the OAM of twisted lights, besides a possible ultrafast generation of skyrmions [45, 46], because a rotating skyrmion manifests itself carrying orbital angular momentum [26, 47]. In the following, we address this idea both theoretically and numerically.

III. THEORETICAL CONSIDERATION BASED ON THIELE EQUATION

We consider an isolated Néel skyrmion whose spin texture is illustrated in Fig. 1 (Bloch skyrmions and antiskyrmions are also interesting). Magnetization dynamics generally is modeled by the Landau-Lifshitz-Gilbert (LLG) equation [48]:

$$\frac{\partial \mathbf{m}}{\partial t} = -\gamma \mathbf{m} \times \mathbf{B}_{\text{eff}} + \alpha \mathbf{m} \times \frac{\partial \mathbf{m}}{\partial t}, \quad (2)$$

where $\mathbf{m} = \mathbf{M}/M_s$ is the magnetization unit vector with saturation magnetization M_s , γ is the gyromagnetic ratio, $\alpha \ll 1$ is the Gilbert damping constant, and \mathbf{B}_{eff} is the local effective field consisting of isotropic exchange coupling, uniaxial anisotropy along z -axis, the interfacial Dzyaloshinskii-Moriya interaction favoring Néel skyrmions, and the optical vortex field (1). Finite temperature effects can be taken into account by including a Gaussian stochastic magnetic field satisfying fluctuation-dissipation theorem [49, 50]. We focus on skyrmion dynamics at zero temperature, if not stated otherwise. The Thiele approach [51, 52] is convenient to derive the analytical solution, where the magnetization dynamics is encoded in the time evolution of the skyrmion position and velocity, $\mathbf{m} = \mathbf{m}(\mathbf{r} - \mathbf{R}(t), \mathbf{V}(t))$ with $\mathbf{R}(t)$ the skyrmion center and $\mathbf{V}(t) = \partial_t \mathbf{R}(t)$ its velocity. We thus obtain

$$-M \partial_t \mathbf{R} + \mathbf{G} \times \partial_t \mathbf{R} - \alpha \mathcal{D} \cdot \partial_t \mathbf{R} + \mathbf{F} = 0, \quad (3)$$

where M multiplying $M_s d/\gamma$ is the effective skyrmion mass originating from the skyrmion deformation and/or dissipation [53, 54], d is the thickness of the film, $\mathbf{G} = -4\pi Q \mathbf{z}$ is the gyromagnetic coupling vector with the skyrmionic topological charge

$Q = (1/4\pi) \int \mathbf{m} \cdot (\partial_x \mathbf{m} \times \partial_y \mathbf{m}) dx dy$, $\mathcal{D}_{ij} = (1/4\pi) \int (\partial_i \mathbf{m} \cdot \partial_j \mathbf{m}) dx dy$ is the dissipative force tensor, and $\mathbf{F} = -\delta\mathcal{H}/\delta\mathbf{R}$ is the driving force with H the total magnetic energy/Hamiltonian [55]. In general, the force \mathbf{F} includes the coupling between the skyrmion with both the optical field and the rotating flower-like magnetization profile (see Fig. 1). Obtaining the analytical expression of the effective force is obviously extremely difficult. As a first approximation, we assume that the skyrmion-flower coupling can be included into the effective skyrmion mass \mathcal{M} and that only the optical field contributes to the effective force. We then arrive at a simple expression $\mathbf{F} = -\int \nabla \mathbf{m} \cdot \mathbf{x} \text{Re}(B_{n,l}) dx dy$. The value of Q depends on the detailed spin profile, e.g. $Q = +1$ for the skyrmion shown in Fig. 1. If $\mathbf{G} \neq 0$, the Lorentz-like force is much larger than the dissipative one. We thus can ignore the friction in (3), and obtain the gyration velocity of the skyrmion $\mathbf{V} = V\hat{\phi}$ with V satisfying

$$\frac{MV^2}{R} + 4\pi QV + F_r = 0, \quad (4)$$

where R is the gyration radius of skyrmion, i.e., the distance from the skyrmion to the optical vortex center, and F_r is the radial component of the driving force. Equation (4) has two circular modes with frequencies $\Omega_{\pm}/2\pi = -Q/M \pm \sqrt{(Q/M)^2 - F_r/(4\pi^2 MR)}$. The friction term in (3) then can be treated perturbatively, which leads to a small velocity correction along the radial direction $\delta\mathbf{v} = -\alpha DV/(4\pi Q + MV/R)\hat{\rho}$. In the perturbative calculation, we have assumed a constant R . However, the restoring force \mathbf{F} may slow down this radial velocity $\delta\mathbf{v}$ as R varies, and thus leads to a radial oscillation (shown in the numerical simulations below).

We emphasize that the predicted rotational motion is not from the geometric confinement due to boundary edges [56–58] of the film, but from the optical trapping and OAM transfer. A spatially homogeneous time-oscillating field considered by Moon *et al.* [58] can induce an unidirectional skyrmion motion with a helical trajectory, where the skyrmion Hall effect was not avoided. Here, the skyrmion gyrates locally around the optical vortex center, instead of either unidirectionally or along device edges, thus in principle avoiding accumulation or annihilation by boundaries.

IV. MICROMAGNETIC SIMULATIONS

To demonstrate the time evolution of the skyrmion motion, we solved numerically the full LLG Eq. (2) using the micromagnetic simulation codes MuMax3 [59–62]. We used magnetic parameters for Pt/Co/AlO_x system with an exchange constant $A = 15$ pJ m⁻¹, a uniaxial anisotropy $K_z = 0.8$ MJ m⁻³, a saturation magnetization $M_s = 0.58$ MA m⁻¹, a Dzyaloshinskii-Moriya constant $D = 3.5$ mJ m⁻², and a Gilbert damping $\alpha = 0.01$. The skyrmion radius r_{sk} is about 10 nm. Materials supporting skyrmions with a larger radius and a stronger thermal stability at room temperature are also interesting. For the majority of results presented in this paper, we consider a ferromagnetic thin film with length 200 nm, width 200 nm and thickness 1 nm, which was discretized using $100 \times 100 \times 1$ finite difference cells. The spin Hamiltonian in the lattice is then $\mathcal{H} = -A'\sum_{\langle i,j \rangle} \mathbf{m}_i \cdot \mathbf{m}_j - D'\sum_{\langle i,j \rangle} (\mathbf{m}_i \times \mathbf{m}_j) \cdot \mathbf{z} - K'_z \sum_i (\mathbf{m}_i \cdot \mathbf{z})^2 - M_s \sum_i \mathbf{B}_{n,l,i} \cdot \mathbf{m}_i$, where \mathbf{m}_i is the unit magnetization vector at i site, $\langle i, j \rangle$ runs over the nearest neighborings, with parameters $A' = 187.5$ meV, $D' = 87.5$ meV, and $K'_z = 40$ meV in lattices. In the simulations, we consider simple optical vortices with $n = 1$. Each B field has one zero at $\rho = \rho_0$ (besides $\rho = 0$) and two local extremums at $\rho = \rho_1$ and ρ_2 ($0 < \rho_1 < \rho_0 < \rho_2$). The field gradient at $\rho = \rho_0$ increases sharply with increasing index l (see Appendix for Fig. 5). In order to reduce the skyrmion deformation caused by the twisted light, we place the skyrmion initially at the zero point $\rho = \rho_0$ of the optical field. We note that, in general, the magnetic/optical constraint works very well when we initially put the skyrmion in the region ($0 < \rho_1 < \rho < \rho_2$). We set $w = 10$ nm (cf. wavelength $\lambda \sim 10$ cm for GHz microwaves in vacuum). We should point out that the width of the light-beam waist w usually cannot be smaller than a half of the wavelength of light due to the diffraction limit. However, thanks to the plasmonics techniques [63, 64], it is possible to achieve focused twisted light with beam width much smaller than the wavelength [65, 66]. On the other hand, although it is computationally too expensive to simulate the gyration of nano-scale skyrmions driven by centimeter-scale microwave vortices if the diffraction barrier is respected, the present results can transfer to those large scales by a proper scaling of the topological charge l with respect to the optical vortex size w based on an angular momentum conservation argument: The dissipation rate of the OAM of a rotating skyrmion is $\alpha D\mathbf{R} \times \partial_t \mathbf{R}$ which should be compensated by optical vortices with OAM $l\hbar$ per photon [This can be proved by taking a cross product with \mathbf{R} at both sides of Eq. (3)]. So, one should keep $l \propto R$ to maintain comparable skyrmion rotation velocities when a much wider beam ($w \sim R$) is used. Numerical results below justifies this argument.

In Figs. 2(a1)-(a9), we show an anticlockwise rotation of the skyrmion about the beam center due to an application of an optical vortex with OAM quantum number $l = +5$, frequency $f = \omega/2\pi = 1$ GHz, and coefficient $B_0 = 10^{-4}$ T m^{1/2} corresponding to a peak magnetic field 1.7 T of the optical vortex. The initial distance ρ_0 between the skyrmion and the optical vortex center is about 20 nm. We find quite a stable skyrmion rotation with negligibly small fluctuations in both the radius and shape (see Visualization 1) indicating a nearly massless skyrmion. The period of rotation is about 6 ns. The linear velocity of the skyrmion V_+ is close to -34.6 m s⁻¹ (positive velocity is defined for clockwise rotation). The velocity is comparable to that achieved by

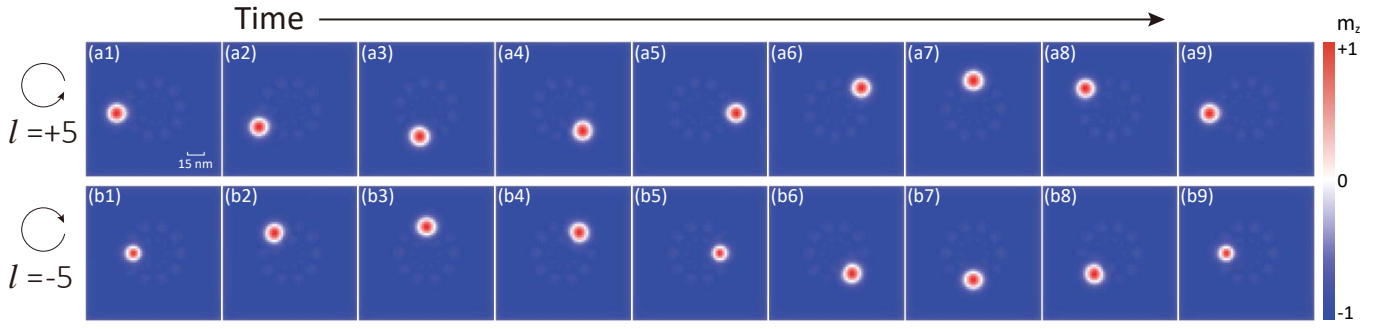


FIG. 2: Time evolution of an isolated Néel skyrmion under optical vortices with OAM quantum number $l = +5$ (a1)-(a9) and $l = -5$ (b1)-(b9). The time intervals between successive snapshots in two cases are 0.8 ns and 0.5 ns, respectively. A positive (negative) topological charge induces an anticlockwise (clockwise) rotation of a skyrmion around the beam axis.

spin-polarized currents with electrical current density of 10^{10} A m $^{-2}$ [3]. The radius of gyration $R_+ \approx 33$ nm is larger than ρ_0 , because the viscous drag δv is outward in the presence of a negative gyration velocity. This stable skyrmion rotation can survive at finite temperatures up to 200 K, without obvious velocity reduction (see Appendix for finite temperature simulations and Fig. 6).

To prove that the rotational motion is indeed due to the OAM transfer from optical vortices to the skyrmion, we provide two more numerical evidences: (i) we reverse the helicity of the optical vortex from $l = +5$ to $l = -5$ without changing the rest parameters. Figures 2(b1)-(b9) demonstrate a striking reversal of the rotation direction of skyrmions, as expected. The rotation period becomes 4 ns. The linear velocity V_- of the skyrmion is estimated to be 31 m s $^{-1}$, with a compressed radius of gyration $R_- \approx 19.7$ nm slightly smaller than ρ_0 since the viscous drag δv now becomes inward. An interesting skyrmion breathing, i.e., skyrmion radius regularly expands and contracts, is found. The observed asymmetry between $|V_+|$ and $|V_-|$ can be well explained by the effective skyrmion mass. From Eq. (4), we derive the emerging skyrmion mass by equating MV_-^2/R_- with $4\pi Q(-V_+ - V_-)$, assuming $F_r(l = 5) \approx -F_r(l = -5)$. After including the coefficient $M_s d/\gamma = 3.3 \times 10^{-15}$ J s m $^{-2}$, we evaluate the skyrmion mass $M \approx 3.06 \times 10^{-24}$ kg. To demonstrate the robustness of the optical confinement, we have tested the case that the skyrmion carries a finite initial velocity achieved by applying an in-plane spin polarized electric current. We find that a small initial velocity, e.g., 16.7 m/s (driven by a current with density 2×10^{11} A/m 2), cannot destroy the magnetic constraint. To test this issue further, we increase the current density up to 2×10^{13} A/m 2 , and still find a very nice magnetic constraint. This can be related to the fact that the skyrmion mass is so small that its inertial effect does not play a key role to overcome the optical trapping. (ii) There still exists a loophole in the above analysis that the skyrmion is probably just interacting with the moving potential minima (the rotating flower) created by the spatially inhomogeneous field. In order to close this loophole, we cut the film into a very narrow annular plate to exclude the effect from the rotating magnetization flower. We observe a fast skyrmion rotation in the confined annular geometry (see Visualization 2 and the Appendix for Fig. 7). This is a direct evidence to justify our understanding. We also note that switching Q from +1 to -1, i.e., spins in the skyrmion core pointing down surrounded by background spins pointing up, does not reverse the handedness of skyrmion rotation. This can be understood that both the driving force F and skyrmionic topological charge Q are odd functions of the magnetization \mathbf{m} , which thus remains the handedness of the rotation identical for opposite Q , cf. Eq. (4). This unique feature has motivated us to apply the present idea to skyrmions in antiferromagnets [67, 68] which usually operate in terahertz (THz) ranges, because an antiferromagnetic skyrmion can be regarded as a superposition of two ferromagnetic skyrmions with antiparallel spins and opposite topological charges. We indeed numerically observed a much faster antiferromagnetic skyrmion rotation with an extremely high velocity ~ 1000 m s $^{-1}$ driven by THz optical vortices (see Visualization 3 and the Appendix for the parameters used in the simulation).

The rotation velocity of skyrmions as a function of the driving frequency ω is shown in Fig. 3(a). The velocity linearly increases with the frequency below 1.5 GHz and sharply decreases then. The peak is due to the resonance between the skyrmion circular frequency Ω_+ and the vortex frequency ω . Higher frequency indicates more diluted photon number density $\propto B_0^2/\omega$, thus reducing the OAM transfer and lowering the skyrmion velocity drastically. Figure 3(b) shows the OAM dependence of the skyrmion velocity, in which we fix the frequency at 1 GHz and choose a coefficient $B_0 = 6 \times 10^{-5}$ T m $^{1/2}$ [69]. The skyrmion velocity is shown to be sensitive to l . At $l = +6$, the breathing skyrmion moves outward due to the radial drag and breaks down when approaching the position $\rho = \rho_2$ where the magnetic field of the optical vortex reaches its local extremum which is so strong to annihilate skyrmions (see Visualization 4). However, this annihilation does not happen for smaller $l (< 6)$ because the magnitude of the vortex field is too weak. Larger $l (> 6)$ sustains a stable skyrmion rotation because skyrmions are pulled back by strong restoring forces (radial field gradients) before they hit the local maximum at $\rho = \rho_2$. A generic criteria to this instability is that the discriminant $\Delta = (2\pi Q)^2 - F_r M/R$ becomes negative which allows no real solutions of Eq. (4). For $l > 6$,

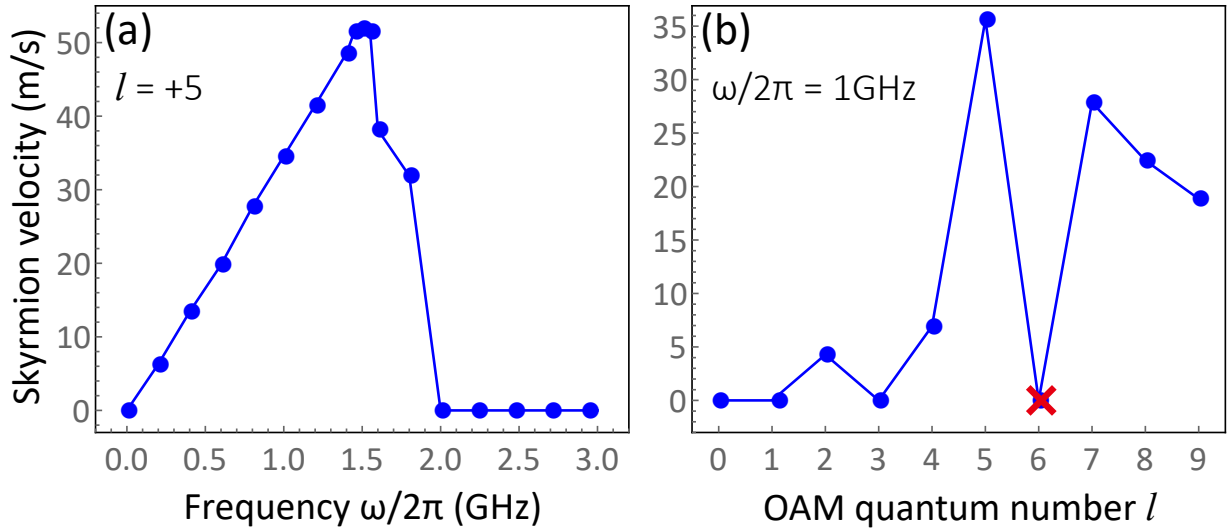


FIG. 3: Skyrmion velocity as a function of the driving frequency (a) and the topological charge (b) of optical vortices. The red cross stamps a skyrmion annihilation. The minus sign of the velocity is dropped.

the skyrmion annihilation does not happen because the corresponding F_r is actually much smaller than the one at $l = +6$. This interpretation is based on analyzing the profile of the optical vortex field $B_{n,l}(\rho)$ plotted in Fig. 5, which has been discussed at the beginning of this session. In our model, the coupling strength between skyrmions and the magnetic profile of the light solely depends on the Zeeman interaction. Since the optical vortex field is non-uniformly distributed in space, the coupling strength varies for different skyrmion position with respect to the beam axis, and for different profile of optical fields as well. The skyrmion velocity dependence on l calculated above indeed changes quantitatively if B_0 (amplitude of light) and w (waist width) are different, while the driving mechanism is essentially the same. A thorough investigation on skyrmion annihilations process will be presented elsewhere.

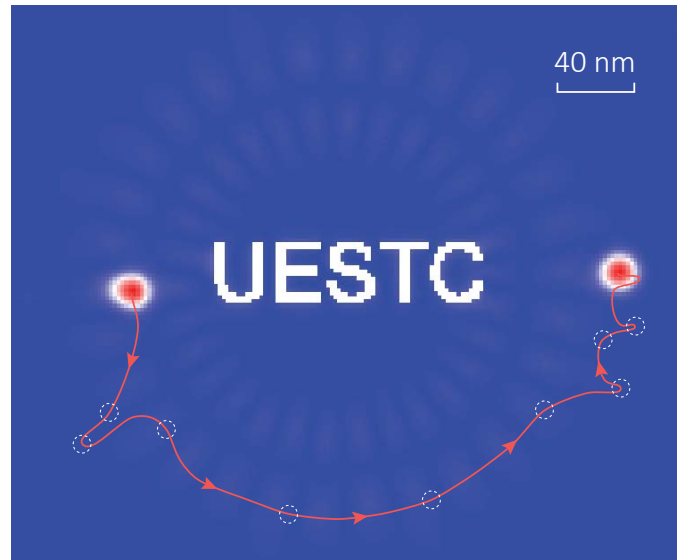


FIG. 4: Skyrmion overflies patterned antidots. The red curve represents the trajectory of the skyrmion with arrows indicating its moving direction. Small white dashed circles are snapshots of the skyrmion. It takes 11.5 ns to deliver the skyrmion from left to the right.

Another merit of our proposal is that a proper design of the gyration orbit can enable skyrmions to bypass defects in magnetic films. To this end, we numerically show how optical vortices can displace magnetic skyrmions across a long distance to overfly patterned antidots (no materials) forming a picture UESTC (white holes in blue magnetic region shown in Fig. 4) on the film of size $400 \text{ nm} \times 400 \text{ nm} \times 1 \text{ nm}$. Here UESTC stands for the abbreviation of the institute of the authors (It can be replaced

by other patterns). We consider a beam with a larger width $w = 35$ nm and an enhanced OAM quantum number $l = +15$. A successful flight for skyrmions without being captured by the holes is observed, despite of a somewhat lingering process due to the competition between the viscous drag induced radial oscillation and the gyration motion (see [Visualization 5](#)). The average rotation velocity of the skyrmion is 50 m s^{-1} , which quantitatively supports the earlier argument on how to transfer our results to a larger length scale. If the defects/barriers are placed in the light-induced magnetic profile, rather than the beam center, one may expect that the field strength of the optical vortex should be large enough to help the skyrmion bypass them. Numerical simulations indeed demonstrate this point (not shown).

V. CONCLUSION

In summary, we proposed an all-photon orbital angular momentum transfer mechanism to manipulate magnetic skyrmions. This OAM transfer can effectively drive the skyrmion rotation around the beam axis. Optical vortices like tweezers are capable of gripping the skyrmion to overfly large-scale barriers without being trapped. The mechanism applies not only to ferromagnetic skyrmions but also to antiferromagnetic ones. Our proposal opens the door for all-optical manipulations of magnetic skyrmions by harvesting the OAM of twisted lights and raises the challenge to generate micron-/submicron-focused optical vortices. Other types of vortex beams such as electron vortices [70, 71] and their acoustic counterparts [72, 73] without breaking the diffraction limit are also promising candidates to drive skyrmion rotations via magnetoelectric and magnetoelastic couplings, respectively. These should be interesting subjects for future research.

VI. APPENDIX

This appendix consists of four parts: The first one shows the spatial distribution of the optical vortex field, the second one details the description of 5 visualizations, the third one calculates the finite temperature effect on the optical vortex driven skyrmion motion, and the last one discusses the skyrmion motion in a narrow annulus.

A. Optical vortex fields

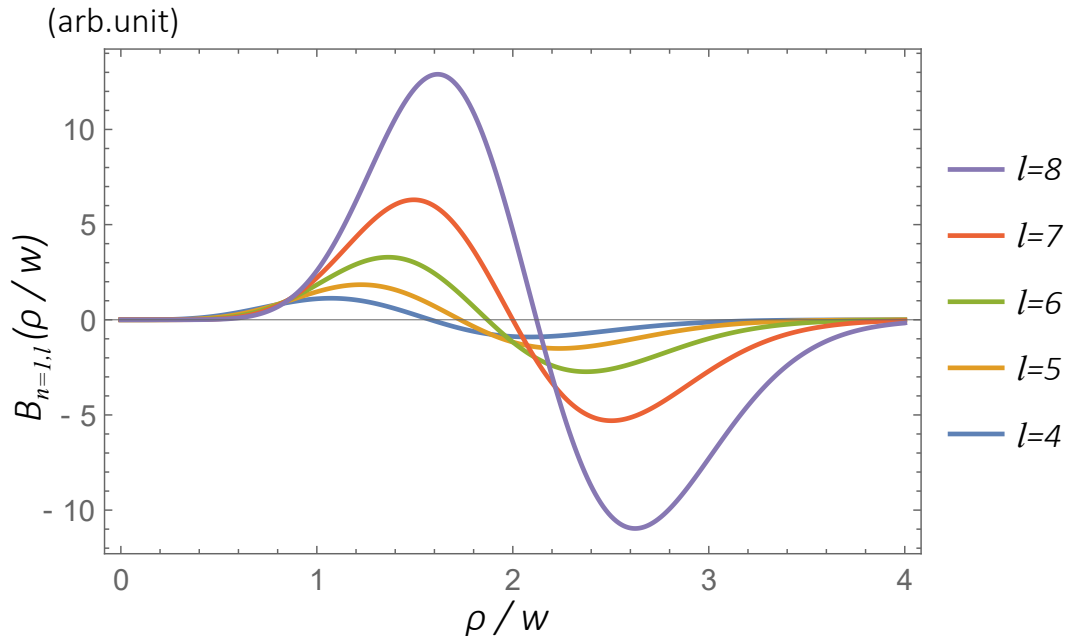


FIG. 5: Spatial profile of the optical vortex field $B_{n,l}(\rho)$ with $n = 1$ for different index l .

As shown in Fig. 5, each B field has one zero at $\rho = \rho_0$ (besides $\rho = 0$) and two local extremums at $\rho = \rho_1$ and ρ_2 ($0 < \rho_1 < \rho_0 < \rho_2$). The field gradient at $\rho = \rho_0$ increases sharply with increasing index l .

B. Visualizations

We describe the five visualizations in detail below.

Visualization 1: Ferromagnetic skyrmion rotation driven by the optical vortex with OAM quantum number $l = +5$ under frequency $f = \omega/2\pi = 1$ GHz and coefficient $B_0 = 10^{-4} \text{ T m}^{1/2}$. The beam waist width is $w = 10$ nm.

Visualization 2: Optical vortex driven skyrmion motion in a narrow annular plate (shown in Fig. 7).

Visualization 3: To perform simulations of optical vortex driven antiferromagnetic skyrmion motion, we use the material parameters for antiferromagnet KMnF_3 (see Ref. [67] in the main text), with the parameters as follows: lattice constant $a = 0.5$ nm, saturation magnetization $M_s = 0.376 \text{ MA m}^{-1}$, antiferromagnetic exchange constant $A = -6.59 \text{ pJ m}^{-1}$, uniaxial anisotropy $K_z = 0.116 \text{ MJ m}^{-3}$, Dzyaloshinskii-Moriya constant $D = 0.7 \text{ mJ m}^{-2}$, and a Gilbert damping $\alpha = 0.01$. We consider a film of size $150 \text{ nm} \times 150 \text{ nm} \times 0.5 \text{ nm}$. The mesh size for the simulations is 0.5 nm . The applied THz optical vortex carries OAM quantum number $l = -10$, frequency $f = 2 \text{ THz}$, waist width $w = 10 \text{ nm}$, and $B_0 = 1 \times 10^{-5} \text{ T m}^{1/2}$. In the simulation, we set a fixed time step $\Delta t = 10 \text{ fs}$.

Visualization 4: Ferromagnetic skyrmion annihilation process by an optical vortex with OAM quantum number $l = +4$ and $B_0 = 7 \times 10^{-5} \text{ T m}^{1/2}$ in a larger ferromagnetic film of size $400 \text{ nm} \times 400 \text{ nm} \times 1 \text{ nm}$.

Visualization 5: Optical vortices displace ferromagnetic skyrmions to overfly patterned antidots (no materials) UESTC (white holes in blue magnetic region) on the two-dimensional ferromagnetic film of size $400 \text{ nm} \times 400 \text{ nm} \times 1 \text{ nm}$. The applied optical vortex carries OAM quantum number $l = +15$ with frequency $f = 1 \text{ GHz}$, width $w = 35 \text{ nm}$, and coefficient $B_0 = 3.3 \times 10^{-8} \text{ T m}^{1/2}$. The maximal magnetic field of the optical vortex is 1.29 T . Center of the beam coincides with that of the patterned antidots.

C. Finite temperature calculations

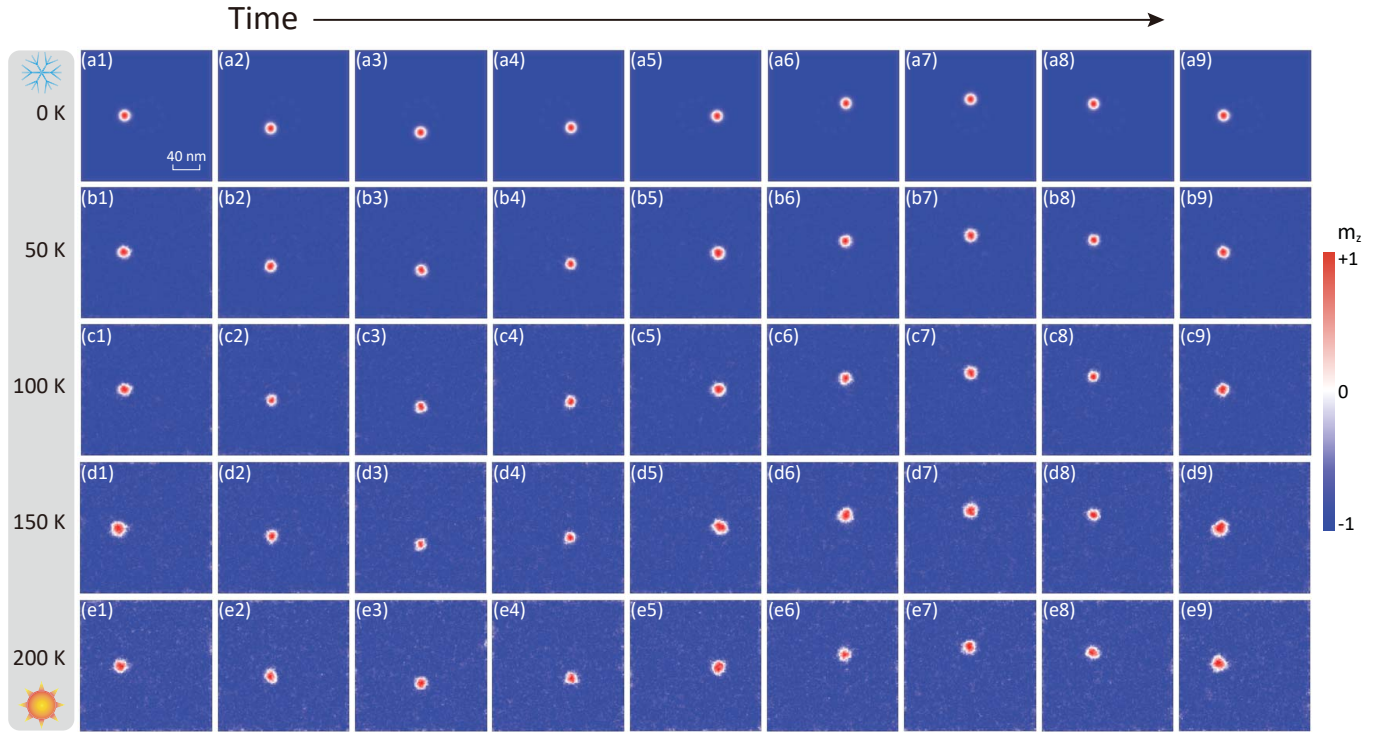


FIG. 6: Time evolution of a Néel skyrmion driven by an optical vortex with $l=+5$ at different temperatures. The time interval between successive snapshots for each temperature is 0.8 ns .

All numerical data presented in the main text are calculated at zero temperature. Here, we take finite temperatures into account

by introducing a Gaussian stochastic magnetic field \mathbf{h} satisfying fluctuation-dissipation theorem

$$\langle h_i(\mathbf{r}, t) h_j(\mathbf{r}', t') \rangle = \frac{2\alpha k_B T}{\gamma M_s \Delta V} \delta(\mathbf{r} - \mathbf{r}') \delta_{ij} \delta(t - t') \quad (5)$$

into the effective field in Eq. (2) in the main text, with k_B the Boltzmann constant, T the absolute temperature of thermal bath, and ΔV the volume of the cell.

Without optical vortices, a single skyrmion can survive in the ferromagnetic thin film at temperatures up to $T = 250$ K. In the presence of an optical vortex with OAM quantum number $l = +5$, waist width $w = 10$ nm, frequency $f = \omega/2\pi = 1$ GHz, and coefficient $B_0 = 10^{-4} \text{ T m}^{1/2}$, we find quite a stable skyrmion rotation without obvious reduction of the velocity by increasing the temperature till $T = 200$ K, above which the skyrmion becomes unstable and can be annihilated by strong thermal fluctuations. This proves that the optical OAM transfer mechanism is robust against thermal fluctuations. Figure 6 shows the calculated time evolution of an isolated Néel skyrmion under the optical vortex described above, at five different temperatures: $T = 0$ K in Fig. 6(a1)-6(a9), $T = 50$ K in Fig. 6(b1)-6(b9), $T = 100$ K in Fig. 6(c1)-6(c9), $T = 150$ K in Fig. 6(d1)-6(d9), and $T = 200$ K in Fig. 6(e1)-6(e9).

D. Skyrmion rotation in an annular plate

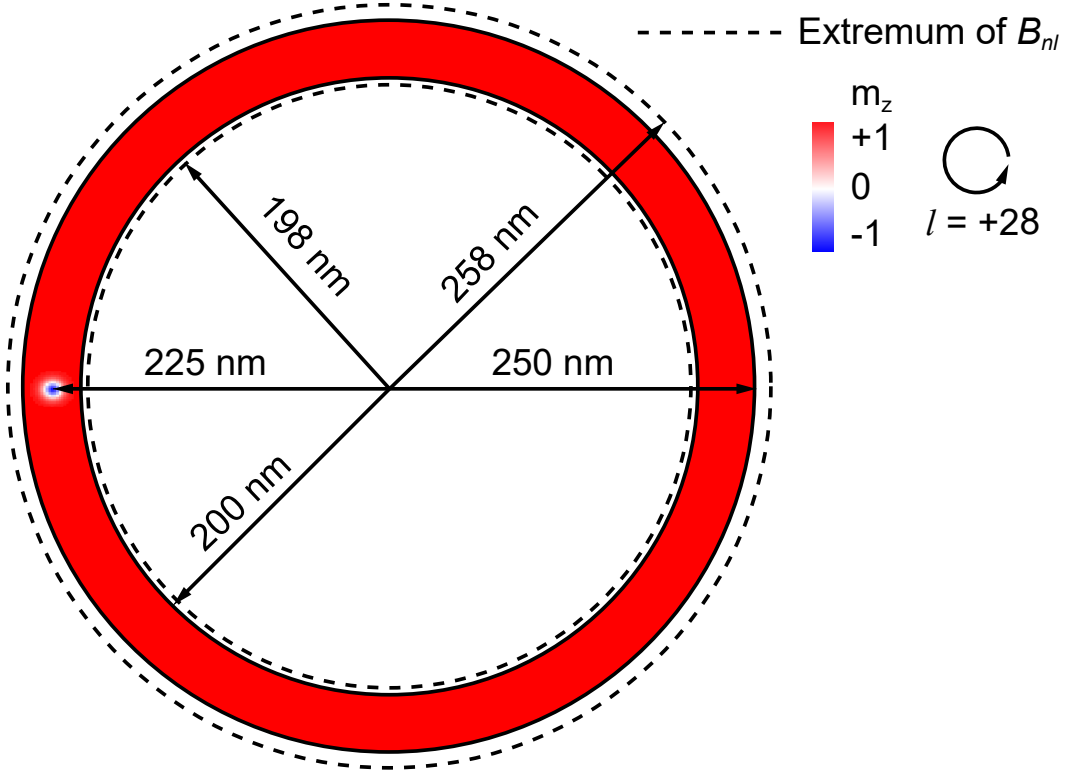


FIG. 7: Geometry of an annular plate confining the skyrmion driven by an optical vortex with $l = +28$.

The ferromagnetic thin film is cut into a very narrow annular plate with inner radius 200 nm and outer radius 250 nm (shown in Fig. 7). The two dashed circles denote the local extremums of the optical vortex with radius $\rho_1 = 198$ nm and $\rho_2 = 258$ nm, respectively. In this annular geometry, we are able to exclude the effect from the rotating flower-like magnetization profile (or the moving potential minimum) on the skyrmion motion. In the numerical simulation, we utilize an optical vortex with frequency $f = 1$ GHz, field coefficient $B_0 = 4.0 \times 10^{-15} \text{ T m}^{1/2}$, waist width $w = 60$ nm, $n = 1$, and OAM quantum number $l = +28$. We use a mesh size $1 \text{ nm} \times 1 \text{ nm} \times 1 \text{ nm}$. A fixed/pinned boundary condition is adopted for spins at both the inner and the outer edges. The observed period of skyrmion rotation is about 29 ns with an average velocity 48.7 m s^{-1} along the orbit of radius 225 nm (see Visualization 2). We thus provide a strong and direct evidence to support our claim of all-photonic orbital angular momentum transfer effect.

Funding

National Natural Science Foundation of China (Grants No. 11604041 and 11704060); the National Key Research Development Program under Contract No. 2016YFA0300801; the National Thousand-Young-Talent Program of China.

Acknowledgments

We thank H.Y. Yuan and Z.Y. Wang for useful discussions.

* Corresponding author: yunshan.cao@uestc.edu.cn

† Corresponding author: yan@uestc.edu.cn

- [1] T.H.R. Skyrme, "A unified field theory of mesons and baryons," *Nucl. Phys.* **31**, 556-569 (1962).
- [2] N. Nagaosa and Y. Tokura, "Topological properties and dynamics of magnetic skyrmions," *Nat. Nanotech.* **8**(12), 899-911 (2013).
- [3] A. Fert, V. Cros, and J. Sampaio, "Skyrmions on the track," *Nat. Nanotech.* **8**(3), 152-156 (2013).
- [4] J. Sampaio, V. Cros, S. Thiaville, and A. Fert, "Nucleation, stability and current-induced motion of isolated magnetic skyrmions in nanostructures," *Nat. Nanotech.* **8**(11), 839-844 (2013).
- [5] J. Iwasaki, M. Mochizuki, and N. Nagaosa, "Current-induced skyrmion dynamics in constrained geometries," *Nat. Nanotech.* **8**(10), 742-747 (2013).
- [6] F. Buttner, C. Moutafis, M. Schneider, B. Kruger, C.M. Gunther, J. Geilhufe, C.v. Korff Schmising, J. Mohanty, B. Pfau, S. Schaffert, A. Bisig, M. Foerster, T. Schulz, C.A.F. Vaz, J.H. Franken, H.J.M. Swagten, M. Klaui, and S. Eisebitt, "Dynamics and inertia of skyrmionic spin structures," *Nat. Phys.* **11**(3), 225-228 (2015).
- [7] N. Romming, A. Kubetzka, C. Hanneken, K. von Bergmann, and R. Wiesendanger, "Field-Dependent Size and Shape of Single Magnetic Skyrmion," *Phys. Rev. Lett.* **114**, 177203 (2015).
- [8] W. Jiang, P. Upadhyaya, W. Zhang, G. Yu, M.B. Jungfleisch, F.Y. Fradin, J.E. Pearson, Y. Tserkovnyak, K.L. Wang, O. Heinonen, S.G.E. te Velthuis, and A. Hoffmann, "Blowing magnetic skyrmion bubbles," *Science* **349**(6245), 283-286 (2015).
- [9] S. Mulbauer, B. Binz, F. Jonietz, C. Pfleiderer, A. Rosch, A. Neubauer, R. Georgii, and P. Boni, "Skyrmion lattice in a chiral magnet," *Science* **323**(5916), 915-919 (2009).
- [10] X.Z. Yu, Y. Onose, N. Kanazawa, J.H. Park, J.H. Han, Y. Matsui, N. Nagaosa, and Y. Tokura, "Real-space observation of a two-dimensional skyrmion crystal," *Nature* **465**(7300), 901-904 (2010).
- [11] S. Heinze, K. von Bergmann, M. Menzel, J. Brede, A. Kubetzka, R. Wiesendanger, G. Bihlmayer, and S. Blugel, "Spontaneous atomic-scale magnetic skyrmion lattice in two dimensions," *Nat. Phys.* **7**(9), 713-718 (2011).
- [12] A.K. Nayak, V. Kumar, T. Ma, P. Werner, E. Pippel, R. Sahoo, F. Damay, U.K. Röbler, C. Felser, and S.S.P. Parkin, "Magnetic anti-skyrmions above room temperature in tetragonal Heusler materials," *Nature* **548**(7669), 561-566 (2017).
- [13] J. Zang, M. Mostovoy, J.H. Han, and N. Nagaosa, "Dynamics of Skyrmion Crystals in Metallic Thin Films," *Phys. Rev. Lett.* **107**, 136804 (2011).
- [14] S.-Z. Lin, C. Reichhardt, C.D. Batista, and A. Saxena, "Driven Skyrmions and Dynamical Transitions in Chiral Magnets," *Phys. Rev. Lett.* **110**, 207202 (2013).
- [15] J. Iwasaki, M. Mochizuki, and N. Nagaosa, "Universal current-velocity relation of skyrmion motion in chiral magnets," *Nat. Commun.* **4**, 1463 (2013).
- [16] H.Y. Yuan and X.R. Wang, "Skyrmion Creation and Manipulation by Nano-Second Current Pulses," *Sci. Rep.* **6**, 22638 (2016).
- [17] R. Wiesendanger, "Nanoscale magnetic skyrmions in metallic films and multilayers: a new twist for spintronics," *Nat. Rev. Mater.* **1**(7), 16044 (2016).
- [18] K. Everschor, M. Garst, B. Binz, F. Jonietz, S. Muhlbauer, C. Pfleiderer, and A. Rosch, "Rotating skyrmion lattices by spin torques and field or temperature gradients," *Phys. Rev. B* **86**, 054432 (2012).
- [19] Y.-H. Liu, Y.-Q. Li, and J.H. Han, "Skyrmion dynamics in multiferroic insulators," *Phys. Rev. B* **87**, 100402 (2013).
- [20] W. Wang, M. Beg, B. Zhang, W. Kuch, and H. Fangohr, "Driving magnetic skyrmions with microwave fields," *Phys. Rev. B* **92**, 020403(R)(2015).
- [21] L. Kong and J. Zang, "Dynamics of an Insulating Skyrmion under a Temperature Gradient," *Phys. Rev. Lett.* **111**, 067203 (2013).
- [22] S.-Z. Lin, C.D. Batista, C. Reichhardt, and A. Saxena, "ac Current Generation in Chiral Magnetic Insulators and Skyrmion Motion induced by the Spin Seebeck Effect," *Phys. Rev. Lett.* **112**, 187203 (2014).
- [23] M. Mochizuki, X.Z. Yu, S. Seki, N. Kanazawa, W. Koshibae, J. Zang, M. Mostovoy, Y. Tokura, and N. Nagaosa, "Thermally driven ratchet motion of a skyrmion microcrystal and topological magnon Hall effect," *Nat. Mater.* **13**(3), 241-246 (2014).
- [24] P. Yan, X.S. Wang, and X.R. Wang, "All-Magnonic Spin-Transfer Torque and Domain Wall Propagation," *Phys. Rev. Lett.* **107**, 177207 (2011).
- [25] J. Iwasaki, A.J. Beekman, and N. Nagaosa, "Theory of magnon-skyrmion scattering in chiral magnets," *Phys. Rev. B* **89**, 064412 (2014).
- [26] C. Schutte and M. Garst, "Magnon-skyrmion scattering in chiral magnets," *Phys. Rev. B* **90**, 094423 (2014).
- [27] Y.-T. Oh, H. Lee, J.-H. Park, and J.H. Han, "Dynamics of magnon fluid in Dzyaloshinskii-Moriya magnet and its manifestation in magnon-Skyrmion scattering," *Phys. Rev. B* **91**, 104435 (2015).

- [28] W. Jiang, X. Zhang, G. Yu, W. Zhang, X. Wang, M.B. Jungfleisch, J.E. Pearson, X. Cheng, O. Heinonen, K.L. Wang, Y. Zhou, A. Homann, and S.G.E. te Velthuis, "Direct observation of the skyrmion Hall effect," *Nat. Phys.* **13**(2), 162-169 (2016).
- [29] K. Litzius, I. Lemesch, B. Kruger, P. Bassirian, L. Caretta, K. Richter, F. Buttner, K. Sato, O.A. Tretiakov, J. Forster, R.M. Reeve, M. Weigand, I. Bykova, H. Stoll, G. Schutz, G.S.D. Beach, and M. Klaui, "Skyrmion Hall effect revealed by direct time-resolved X-ray microscopy," *Nat. Phys.* **13**(2), 170-175 (2017).
- [30] X. Zhang, Y. Zhou, and M. Ezawa, "Magnetic bilayer-skyrmions without skyrmion Hall effect," *Nat. Commun.* **7**, 10293 (2016).
- [31] J. Muller and A. Rosch, "Capturing of a magnetic skyrmion with a hole," *Phys. Rev. B* **91**, 054410 (2015).
- [32] C. Reichhardt, D. Ray, and C.J. Olson Reichhardt, "Collective Transport Properties of Driven Skyrmions with Random Disorder," *Phys. Rev. Lett.* **114**, 217202 (2015).
- [33] J. Poynting, "The wave motion of a revolving shaft, and a suggestion as to the angular momentum in a beam of circularly polarised light," *Proc. R. Soc. London A Contain. Pap. Math. Phys. Character* **82**, 560 (1909).
- [34] R.A. Beth, "Direct detection of the angular momentum of light," *Phys. Rev.* **48**, 471 (1935).
- [35] R.A. Beth, "Mechanical detection and measurement of the angular momentum of light," *Phys. Rev.* **50**, 115 (1936).
- [36] L. Allen, M.W. Beijersbergen, R.J. Spreeuw, and J.P. Woerdman, "Orbital angular momentum of light and the transformation of Laguerre-Gaussian laser modes," *Phys. Rev. A* **45**, 8185 (1992).
- [37] I.V. Basistiy, M.S. Soskin, and M.V. Vasnetsov, "Optical wavefront dislocations and their properties," *Opt. Commun.* **119**(5-6), 604-612 (1995).
- [38] D.L. Andrews and M. Babiker, *The Angular Momentum of Light* (Cambridge Univ., 2012).
- [39] A. Nicolas, L. Veissier, L. Giner, E. Giacobino, D. Maxein, and J. Laurat, "A quantum memory for orbital angular momentum photonic qubits," *Nat. Photonics* **8**(3), 234-238 (2014).
- [40] N. Bozinovic, Y. Yue, Y. Ren, M. Tur, P. Kristensen, H. Huang, A.E. Willner, and S. Ramachandran, "Terabit-scale orbital angular momentum mode division multiplexing in fibers," *Science* **340**(6140), 1545-1548 (2013).
- [41] J. Wang, J.-Y. Yang, I.M. Fazal, N. Ahmed, Y. Yan, H. Huang, Y. Ren, Y. Yue, S. Dolinar, M. Tur, and A.E. Willner, "Terabit free-space data transmission employing orbital angular momentum multiplexing," *Nat. Photonics* **6**(7), 488-496 (2012).
- [42] F. Tamburini, B. Thide, G. Molina-Terriza, and G. Anzolin, "Twisting of light around rotating black holes," *Nat. Phys.* **7**(3), 195-197 (2011).
- [43] R. Fickler, G. Campbell, B. Buchler, P.K. Lam, and A. Zeilinger, "Quantum entanglement of angular momentum states with quantum numbers up to 10,010," *PNAS* **113**(48), 13642-13647 (2016).
- [44] The cycle-averaged angular momentum density \mathbf{j} associated with the transverse EM field is shown to be $\mathbf{j} = \epsilon_0 \mathbf{r} \times \langle \mathbf{E} \times \mathbf{B} \rangle$, while the total angular momentum of the field is $\mathbf{J} = \epsilon_0 \int \mathbf{r} \times \langle \mathbf{E} \times \mathbf{B} \rangle d\mathbf{r}$. Here ϵ_0 is the vacuum permittivity and \mathbf{E} is the electric field. For linearly polarized LG modes (1), the OAM density in the direction of propagation is given by $j_z = \epsilon_0 \omega l |B(\mathbf{r})|^2$. The OAM integrated over the beam is shown to be equivalent to $\hbar h$ per photon: $J_z = \hbar h$.
- [45] H. Fujita and M. Sato, "Ultrafast generation of skyrmionic defects with vortex beams: Printing laser profiles on magnets," *Phys. Rev. B* **95**, 054421 (2017).
- [46] H. Fujita and M. Sato, "Encoding Orbital Angular Momentum of Lights in Magnets," arXiv:1612.00176.
- [47] O. Tchernyshyov, "Conserved momenta of a ferromagnetic soliton," *Ann. Phys.* **363**, 98-113 (2015).
- [48] T.L. Gilbert, "A phenomenological theory of damping in ferromagnetic materials," *IEEE Trans. Mag.* **40**(6), 3443-3449 (2004).
- [49] W.F. Brown, Jr., "Thermal Fluctuations of a Single-Domain Particle," *Phys. Rev.* **130**, 1677 (1963).
- [50] P. Yan, G.E.W. Bauer, and H.W. Zhang, "Energy repartition in the nonequilibrium steady state," *Phys. Rev. B* **95**, 024417 (2017).
- [51] A.A. Thiele, "Steady-State Motion of Magnetic Domains," *Phys. Rev. Lett.* **30**, 230 (1973).
- [52] O.A. Tretiakov, D. Clarke, Gia-Wei Chern, Ya.B. Bazaliy, and O. Tchernyshyov, "Dynamics of Domain Walls in Magnetic Nanostrips," *Phys. Rev. Lett.* **100**, 127204 (2008).
- [53] I. Makhfudz, B. Kruger, and O. Tchernyshyov, "Inertia and Chiral Edge Modes of a Skyrmion Magnetic Bubble," *Phys. Rev. Lett.* **109**, 217201 (2012).
- [54] R.E. Troncoso and A.S. Nez, "Brownian motion of massive skyrmions in magnetic thin films," *Ann. Phys.* **351**, 850-856 (2014).
- [55] A.P. Malozemoff and J.C. Slonczewski, *Magnetic Domain Walls in Bubble Materials* (Academic, New York, 1979).
- [56] Y.Y. Dai, H. Wang, P. Tao, T. Yang, W.J. Ren, and Z.D. Zhang, "Skyrmion ground state and gyration of skyrmions in magnetic nanodisks without the Dzyaloshinsky-Moriya interaction," *Phys. Rev. B* **88**, 054403 (2013).
- [57] F. Garcia-Sanchez, J. Sampaio, N. Reyren, V. Cros, and J.-V. Kim, "A skyrmion-based spin-torque nano-oscillator," *New J. Phys.* **18**, 075011 (2016).
- [58] K.-W. Moon, D.-H. Kim, S.-G. Je, B.S. Chun, W. Kim, Z.Q. Qiu, S.-B. Choe, and C. Hwang, "Skyrmion motion driven by oscillating magnetic field," *Sci. Rep.* **6**, 20360 (2015).
- [59] A. Vansteenkiste, J. Leliaert, M. Dvornik, M. Helsen, F. Garcia-Sanchez, and B. Van Waeyenberge, "The design and verification of MuMax3," *AIP Adv.* **4**(10) 107133 (2014).
- [60] S. Pizzini, J. Vogel, S. Rohart, L.D. Buda-Prejbeanu, E. Jué, O. Boulle, I.M. Miron, C.K. Safeer, S. Auffret, G. Gaudin, and A. Thiaville, "Chirality-Induced Asymmetric Magnetic Nucleation in Pt/Co/AIO_x Ultrathin Microstructures," *Phys. Rev. Lett.* **113**, 047203 (2014).
- [61] Y. Zhou, E. Iacocca, A.A. Awad, R.K. Dumas, F.C. Zhang, H.B. Braun, and J. Akerman, "Dynamically stabilized magnetic skyrmions," *Nat. Commun.* **6**, 8193 (2016).
- [62] X. Zhang, M. Ezawa, and Y. Zhou, "Thermally stable magnetic skyrmions in multilayer synthetic antiferromagnetic racetracks," *Phys. Rev. B* **94**, 064406 (2016).
- [63] Y. Gorodetski, A. Niv, V. Kleiner, and E. Hasman, "Observation of the Spin-Based Plasmonic Effect in Nanoscale Structures," *Phys. Rev. Lett.* **101**, 043903 (2008).
- [64] W.L. Barnes, A. Dereux, and T.W. Ebbesen, "Surface plasmon subwavelength optics," *Nature* **424**(6950), 824-830 (2003).

- [65] R.W. Heeres and V. Zwiller, "Subwavelength Focusing of Light with Orbital Angular Momentum," *Nano Lett.* **14**(8), 4598-4601 (2014).
- [66] J.Y. Yin, J. Ren, L. Zhang, H. Li, and T.J. Cui, "Microwave Vortex-Beam Emitter Based on Spoof Surface Plasmon Polaritons," arXiv:1703.07487.
- [67] J. Barker and O.A. Tretiakov, "Static and Dynamical Properties of Antiferromagnetic Skyrmions in the Presence of Applied Current and Temperature," *Phys. Rev. Lett.* **116**, 147203 (2016).
- [68] X. Zhang, Y. Zhou, and M. Ezawa, "Antiferromagnetic Skyrmion: Stability, Creation and Manipulation," *Sci. Rep.* **6**, 24795 (2016).
- [69] The corresponding maximal magnetic field of the optical vortex is 0.56 T, 0.34 T, 0.35 T, 0.44 T, 0.63 T, 1.06 T, 1.87 T, 3.38 T, 7.61 T, and 16.76 T for $l = 0, 1, 2, \dots$, and 9, respectively.
- [70] A. B ech e, R. Juchtmans, and J. Verbeeck, "Efficient creation of electron vortex beams for high resolution STEM imaging," *Ultramicroscopy* **178**, 12-19 (2017).
- [71] E. Mafakheri, A.H. Tavabi, P.-H. Lu, R. Balboni, F. Venturi, C. Menozzi, G.C. Gazzadi, S. Frabboni, A. Sit, R.E. Dunin-Borkowski, E. Karimi, and V. Grillo, "Realization of electron vortices with large orbital angular momentum using miniature holograms fabricated by electron beam lithography," *Appl. Phys. Lett.* **110**, 093113 (2017).
- [72] Z. Hong, J. Zhang, and B.W. Drinkwater, "Observation of Orbital Angular Momentum Transfer from Bessel-Shaped Acoustic Vortices to Diphasic Liquid-Microparticle Mixtures," *Phys. Rev. Lett.* **114**, 214301 (2015).
- [73] D. Baresch, J.-L. Thomas, and R. Marchiano, "Observation of a Single-Beam Gradient Force Acoustical Trap for Elastic Particles: Acoustical Tweezers," *Phys. Rev. Lett.* **116**, 024301 (2016).